Original Research

Characterizing leaf-deposited particles: Single-particle mass spectral analysis and comparison with naturally fallen particles

Dele Chen [a, b, c], Hua-Yun Xiao [a], Ningxiao Sun [a, b, c], Jingli Yan [a, b, c], Shan Yin [a, b, c, *]

[a] School of Agriculture and Biology, Shanghai Jiao Tong University, 800 Dongchuan Rd., Shanghai 200240, China
[b] Shanghai Yangtze River Delta Eco-Environmental Change and Management Observation and Research Station, Ministry of Science and Technology, Ministry of Education, 800 Dongchuan Rd., Shanghai 200240, China
[c] Shanghai Urban Forest Ecosystem Research Station, National Forestry and Grassland Administration, 800 Dongchuan Rd., Shanghai 200240, China

ARTICLE INFO

ABSTRACT

The size and composition of particulate matter (PM) are pivotal in determining its adverse health effects. It is important to understand PM's retention by plants to facilitate its atmospheric removal. However, the distinctions between the size and composition of naturally fallen PM (NFPM) and leaf-deposited PM (LDPM) are not well-documented. Here we utilize a single-particle aerosol mass spectrometer, coupled with a PM resuspension chamber, to analyze these differences. We find that LDPM particles are 6.8 −97.3 % larger than NFPM. Employing a neural network algorithm based on adaptive resonance theory, we have identified distinct compositional profiles: NFPM predominantly consists of organic carbon (OC; 31.2 %) and potassium-rich components (19.1 %), whereas LDPM are largely composed of crustal species (53.9−60.6 %). Interestingly, coniferous species retain higher OC content (11.5−13.7 %) compared to broad-leaved species (0.5−1.2 %), while the levoglucosan content exhibit an opposite trend. Our study highlights the active role of tree leaves in modifying PM composition beyond mere passive capture, advocating for a strategic approach to species selection in urban greening initiatives to enhance PM mitigation. These insights provide guidance for urban planners and environmentalists in implementing nature-based solutions to improve urban air quality.

1. Introduction

Particulate matter (PM) pollution is a major environmental concern because it can cause severe air quality problems and pose serious threats to public health [1]. Fine and ultrafine particles, especially those at nano sizes (less than 100 nm in diameter), are associated with adverse health effects, such as respiratory and cardiovascular diseases, because they can penetrate deep into the bloodstream and translocate to the lungs [2] or brain [1]. Associations between PM constituents and health effects have been extensively reported. For example, organic carbon (OC), which mainly originates from plants, incomplete combustion, and vehicular emissions, can generate strong oxidative potential [3], bind to cell membranes, interfere with cell metabolism, and cause cell damage [4].

Distinguishing between primary and secondary PM sources is central to ongoing atmospheric research [5]. Primary sources, which include vehicular and industrial emissions, can be identified directly [6]. In contrast, the formation of secondary PM, which is the result of complex atmospheric photochemical reactions, introduces challenges [7]. Advanced analytical techniques have revealed a comprehensive spectrum of PM components, from OC and elemental carbon (EC) to heavy metals (HMs) and crustal species (Crust) [8]. These findings embody the need for tailored air quality management strategies related to the specific PM composition and its primary sources. The epidemiological associations between increased PM levels and adverse respiratory outcomes further emphasize the urgent need for PM mitigation strategies [9].

The process of PM deposition involves the settling of particles from the air onto surfaces and their removal [10], a phenomenon influenced by factors such as land cover and surface properties [11]. Research comparing PM deposition has revealed lower velocities in Beijing's wetlands compared to local forests [12]. However, the

* Corresponding author. School of Agriculture and Biology, Shanghai Jiao Tong University, 800 Dongchuan Rd., Shanghai 200240, China.
E-mail address: yinshan@sjtu.edu.cn (S. Yin).

quantity and composition of PM deposited on a given underlying surface are affected by regional and local sources [13]. For example, vehicle exhaust primarily comprises EC and OC [14], while ambient particles near power plants are rich in silicate and metal fractions [15]. Debates exist regarding whether underlying surfaces passively accumulate PM from all sources or actively capture specific particle types [16,17], but it is clear that the interaction between PM particles and these surfaces during deposition is complex and not fully understood [3].

Recent studies have increasingly focused on the integration of advanced data analytics and modeling techniques to better understand PM dynamics on a larger scale [18]. For instance, research employing big data and machine learning algorithms has been instrumental in mapping and predicting PM distribution patterns in urban areas [19]. By reducing the emission of PM at the source [4], nanotechnology in biodiesel combustion compensates for the hazards of PM pollution [20]. Additionally, there is growing emphasis on the role of urban forests in mitigating PM pollution across cities and countries. Studies in cities such as Beijing [17] and Naples [10] have explored how the strategic placement of green spaces and urban forests can effectively reduce ambient PM levels, thereby contributing to tackling the complex challenges of air quality improvement at the city or country level [18].

Urban buildings and vegetation serve as large underlying surfaces for PM deposition [21]. The surfaces of building facades and rooftops, which are often hard and smooth, influence the quantity of PM deposition [22]. Considerable research has examined the PM capture efficiency of different species by using the vacuum filtration method [23] and conducting modeling [10], yet studies characterizing the size and composition of leaf-deposited particles are scarce (Table 1). Notably, real-time methods are unavailable for determining both the size and composition of PM particles deposited on underlying surfaces. The size distribution and chemical composition of LDPM and comparisons with NFPM remain elusive. The size and composition of PM particles deposited on underlying surfaces might be affected by surface modifications [24]; however, experimental evidence regarding this aspect is lacking.

The emergence of single-particle aerosol mass spectrometry (SPAMS) has enabled the rapid and direct determination of the size and components of individual aerosol particles [34]. SPAMS has been widely applied in the field for monitoring the chemical composition of atmospheric PM and analyzing individual particles in ground dust [35] or in pollution sources such as street canyons [13], power plants [15], wood boilers [2], and highway tunnels [36]. However, SPAMS has not yet been used to characterize single particles on underlying surfaces, mainly because of the difficulty in injecting surface-adhered particles into SPAMS equipment. This difficulty exists because the hard surfaces on which PM is deposited are considerably different from the air. Thus, a resuspension method must be used to convert surface-deposited particles into air-suspended ones for an accurate analysis of these particles.

This study aims to answer the following questions: (1) What is the size distribution and composition spectrum of PM that settles on the surface of leaves? And (2) How do these differ from those of the PM that settles naturally on a hard surface? To answer these questions, an in situ experiment is designed to investigate PM deposition on the leaf surfaces of six tree species and hard trays, with the particle size and chemical composition measured using a self-developed PM resuspension chamber (PMRC) coupled with an SPAMS. A neural network algorithm is used to classify the chemical characteristics of the deposited PM, after which source analysis is performed to determine the source characteristics of the deposited PM. This research offers methodological insights into determining the size and composition of PM on object surfaces. The findings are conducive to the rational allocation of tree species to efficiently remove specific components of PM.

2. Materials and methods

A systematic approach was employed to assess PM deposition and composition, with a focus on the interaction between airborne particles and various tree species. The methodology was meticulously designed to capture the nuances of PM dynamics in an arboretum. The study involved a detailed examination of both NFPM and LDPM from selected broad-leaved and coniferous species, employing advanced techniques for precise measurement and analysis. This included the use of a custom-built PMRC in conjunction with SPAMS to analyze the aerodynamic diameter, chemical composition, and source apportionment of PM. The subsequent data analysis incorporated computational techniques, including the ART-2a algorithm, for an in-depth understanding of particle clustering and compositional categories.

2.1. Study area

This study was performed in a 5.5 ha (55,000 m^2) arboretum at the Minhang Campus of Shanghai Jiao Tong University (31°2′ N, 121°26′ E) in Shanghai, China (Fig. 1). This arboretum contains a mixture of evergreen broad-leaved species and coniferous species. Shanghai has a subtropical monsoon climate, with a mean annual temperature of 18 °C and precipitation of 1100 mm. The mean concentrations of $PM_{2.5}$ and PM_{10} during the experimental period were 7.7 and 12.5 $\mu g\ m^{-3}$, respectively (Fig. S1, Supplementary Materials). The Shanghai−Jinshan Expressway crosses the campus and is located 400 m away from the arboretum, and a thermal

Table 1
Studies characterizing the size and composition of PM accumulated on leaf surfaces.

Category	Parameters	Method	Reference
Size fractions	PM_1, $PM_{2.5}$, PM_{10}	SEM	[23]
	$PM_{2.5}$, PM_{10}	Vacuum filtration	[23]
	$PM_{2.5}$, $PM_{2.5-10}$, PM_{10-100}	Elution-filtration- weighing	[25]
	$PM_{0.2-3}$, PM_{3-10}, PM_{10-100}	Elution-filtration- weighing	[26]
	PM_1, $PM_{1-2.5}$, $PM_{2.5-5}$	Sweep-resuspension- particle size spectrometer	[27]
	Average size	X-ray microscope	[27]
Ion concentrations	Mass fractions of 10 water-soluble ions	IC	[28]
	Concentrations of NO_3^- and SO_4^{2-} in wash-off suspensions	IC	[29]
Elemental compositions	Concentrations of 23 elements (Na, Mg, Al, Si, P, etc.)	SEM/EDX	[30]
	Concentrations of 12 elements (Ca, Mg, P, Al, Si, etc.)	SEM/EDX	[31]
	Concentrations of 16 metal elements (Ba, Cd, Cr, Cs, Cu, etc.)	ICP-MS	[32]
	Concentrations of Cr, Cd, Ni, Cu, and Pb	ICP-OES	[33]

Fig. 1. Overview of the study area. This figure illustrates the location of the arboretum and its surrounding urban features. The sequence of maps narrows from a city-wide scale to a detailed view of the arboretum, highlighting its position relative to local sources of PM, such as the expressway and power plant.

power plant is located approximately 4000 m northeast (Fig. 1).

2.2. Sample collection

Collection of leaf-deposited particles. Before experimentation, a period without precipitation was selected in August to simulate the dry deposition process of atmospheric particles onto tree leaves. The selected species are commonly used for urban greening in Shanghai and many other cities across China. Two are broad-leaved species (*Cinnamomum camphora* and *Magnolia grandiflora*), and the other two are coniferous species (*Taxodium ascendens* and *Sabina chinensis* (L.) Ant. "*Kaizuca*") (Fig. S2, Supplementary Materials). A standardized sampling protocol was followed using the same equipment. Sampling was conducted on three random trees of each species. These trees were healthy and not infested with diseases or pests. Before ambient PM exposure, mature leaf samples (200 and 600 leaves for broad-leaved and coniferous species, respectively) were washed three times in situ using deionized water to remove the originally retained coarse particles. These washed leaves were located at a height of 3 m and were marked (Fig. 2a), and an overlap between the selected leaves was avoided as far as possible. The washed leaves were exposed to an ambient PM environment for seven days (August 1−8, 2021). Subsequently, sampling was conducted at 9 a.m. on a sunny morning under windless conditions. All leaf samples were gently collected into opaque tinfoil bags and then transported to a laboratory immediately for a PM resuspension experiment (Fig. 2b).

Collection of naturally fallen particles. To compare the chemical compositions and size distributions of LDPM with NFPM, particles naturally deposited on hard trays were collected. Sterilized and smooth trays (diameter: 400 mm) were fastened to the roof (height: 3 m) of an observation station in the arboretum to collect NFPM for seven days through dry deposition (Fig. 2a). Replicates of particles on three trays were pooled into a single NFPM sample, placed gently into an opaque tinfoil bag, and taken to the laboratory for PM resuspension and SPAMS analysis (Fig. 2b). A sieve 5 mm in diameter was placed above a tray to prevent the contamination of NFPM by debris from dead branches and leaves and adsorbed particles (Fig. 2a).

2.3. Particulate matter resuspension chamber coupled with single-particle aerosol mass spectrometry

A schematic of the developed PMRC with SPAMS is displayed in Fig. 2b. The PMRC is made of stainless steel and has a size of 0.686 m^3. This chamber has an openable door for sample insertion, inlet and outlet holes for allowing the flow of the carrier gas (N$_2$, 99.9 %), and a stainless steel injection hole for SPAMS measurement. A high-pressure nitrogen container was connected to the chamber. The inner side of the chamber contains a fan to ensure the full exposure of samples to an omnidirectional aerosol flow, and rubber gloves were used by the system operator [37].

The sweep−resuspension process consisted of five steps. First, the inner wall of the chamber was scrubbed with deionized water and ventilated using the carrier gas (N$_2$, 99.9 %) to reduce the background concentration of PM in the chamber to <5 μg m^{-3}, measured using a particle size spectrometer (GRIMM 11-R, Germany). Second, the trays or leaves with PM were placed into the PMRC through the chamber door, and the fans were turned on. Third, the PM deposited on the tray and leaf surfaces was gently swept off and dispersed evenly throughout the ambient environment of the chamber. The fans inside the chamber facilitated PM resuspension over a limited volume. Fourth, the resuspended PM particles were injected into an 8-mm-diameter stainless steel tube connected to the vacuum-pumped inlet of the SPAMS equipment (Hexin Analytical Instrument, China). These particles then passed through a 100-μm critical orifice at a controlled flow of 80 mL min^{-1} (Fig. 2c). Finally, the internal part of the chamber was
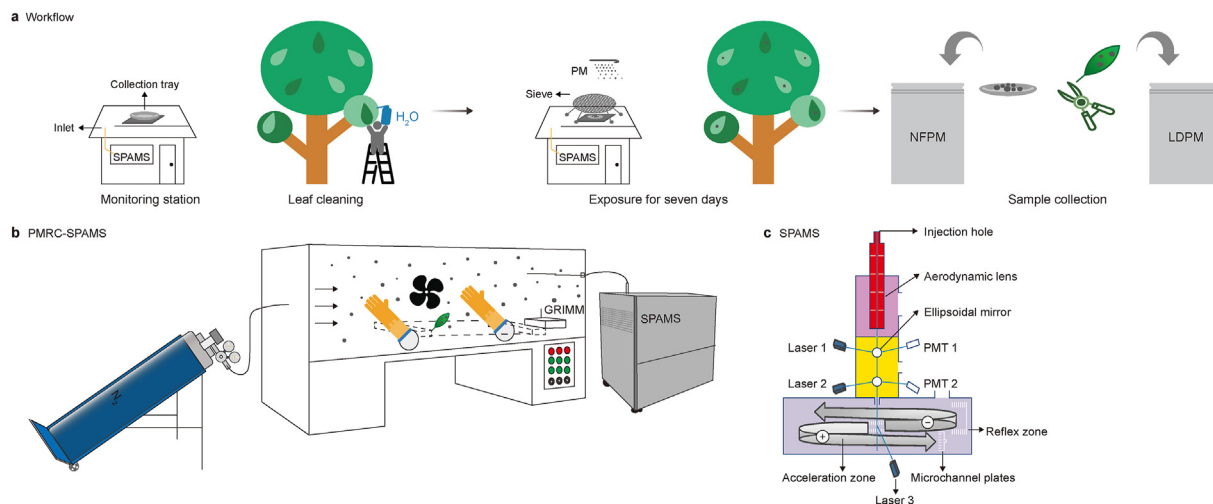
Fig. 2. Schematic of the working flow and experimental setup. **a**, The workflow for monitoring and sample collection, showing the initial cleaning of leaves, their exposure to ambient PM for seven days, and the subsequent collection of NFPM and LDPM into opaque tinfoil bags. **b**, The PM resuspension chamber (PMRC) is linked to the single particle aerosol mass spectrometer (SPAMS) for size and composition analysis of collected samples. **c**, The internal components of SPAMS, highlighting the injection hole, aerodynamic lens, ellipsoidal mirror, laser beams, photomultiplier tubes (PMT), acceleration zone, microchannel plates, and the reflex zone, which together facilitate the precise detection and characterization of PM.

cleaned using N_2 after the completion of the SPAMS analysis to prepare the system for the next sample.

The operating conditions of the PMRC were optimized before the experiment, and the optimized operating parameters were as follows: the N_2 flow rate was 5 L min^{-1}; the wind speed of the fans was 1 m s^{-1}; 50 leaves of broad-leaved species and 150 from coniferous species were randomly selected for PM resuspension; and the time for the SPAMS analysis of one sample was 2 h. In addition, a stainless steel tube was stuck outside the window of the monitoring station at the same height as the fastened tray and marked leaves. Through this tube, atmospheric PM (APM) was introduced into the SPAMS equipment to determine the particle size and chemical composition (Fig. 2a). The SPAMS equipment operated continuously, recording APM measurements for 6–8 h daily during the daytime over the one-week sampling period, aligning with the duration of the LDPM and NFPM collection and analysis.

The working principle of SPAMS was described in a previous study [35]. Briefly, the particles introduced into the aforementioned spectrometer are focused and accelerated to specific velocities based on their aerodynamic diameters while passing through an aerodynamic lens. In the sizing region, the aerodynamic sizes of individual particles are measured using two continuous-diode neodymium-doped yttrium aluminum garnet (Nd:YAG) laser beams with a wavelength of 532 nm. Subsequently, ionization is conducted using a 266-nm Nd:YAG laser beam to produce positive and negative ion fragments [38]. The bipolar mass spectra of a single particle are detected using a dual-polarity, time-of-flight mass spectrometer, and positive- and negative-ion spectra are acquired. In this study, a high-power Nd:YAG laser was used in the spectrometer. The energy of the ionization laser was set to 0.6 mJ [39], and the power density of this laser was relatively low (approximately 1.06×10^8 W cm^{-2}).

2.4. Quality assurance and quality control

Polystyrene latex spheres of standardized sizes (0.23, 0.32, 0.51, 0.73, 0.96, 1.4, and 2.0 μm in diameter; Nanosphere Size Standards, Duke Scientific Corp., Palo Alto) were employed for the calibration of particle size detection in the experiment. Concurrently, specific ions of Li, Na, K, V, Ba, and Pb were utilized for the calibration of the mass spectrum. To prepare the calibration solutions, each set of seven standard polystyrene latex suspensions or the six-metal solution was dissolved in 100 mL of ultrapure water. These solutions were then atomized using an aerosol generator (Model 9032, TSI Inc., USA). The resulting aerosol was directed through a silica gel diffusion dryer and then introduced into SPAMS at a controlled flow rate of 100 mL min^{-1}.

2.5. Data analysis

The particle counts with size information were used to depict the distribution of particle quantities across different sizes for APM, NFPM, and LDPM. The average particle diameter (D_c) was obtained by integrating the fitting curve for each particle size using equation (1).

$$D_c = \frac{\int_{0.1}^{2.5} x \cdot LN_x \, dx}{\int_{0.1}^{2.5} LN_x \, dx}, \tag{1}$$

where x is the particle size and LN_x represents the corresponding PM quantity.

SPAMS enables the acquisition of a substantial amount of data through the sizing and chemical analysis of hundreds or thousands of particles. In the current study, spectral peak thresholds were employed to differentiate signals from background noise. Peaks with a height below 10 units and an area under 20 units were excluded to ensure clarity and accuracy in the signal analysis [13]. The resulting peak data for the ionized particles were analyzed using the SPAMS Data Analysis toolkit V2.2-p (Guangzhou Hexin Instrument Co., Ltd.). In the current analysis, single particles were classified into distinct clusters based on the ion peak patterns in their mass spectra, utilizing the ART-2a algorithm — a type of neural network grounded in adaptive resonance theory [40]. This method is suitable for real-time unsupervised pattern recognition and the categorization of data.

The vigilance factor parameter, set at 0.75, determines the granularity of the clustering, with a higher value leading to finer, more distinct clusters. This setting was chosen based on prior successful applications in single-particle analysis [35,41] to ensure a balance between the specificity and generalizability of the identified particle types. The learning rate influences the speed at which the network learns, and 0.05 was selected to allow the algorithm to converge steadily and avoid overfitting, as suggested by Liu et al. [36]. Lastly, the maximum number of iterations was capped at 20 to limit the computational time while ensuring an adequate opportunity for the algorithm to stabilize on a solution.

The ART-2a area matrix of a particle cluster represents the average peak intensity for particles with a certain mass-to-charge ratio (m/z) and, thus, mirrors the typical mass spectrum of these particles. The ART-2a algorithm produced multiple clusters to describe the datasets. The detailed ART-2a-based classification method is described in the Supplementary text. The mass spectra similarities between the generated clusters were manually examined, and clusters with similar spectra were subsequently merged into typical component categories. Hierarchical cluster analysis was performed to cluster the samples using the K-means algorithm based on the average linkage method.

3. Results and discussion

In this study, for the in situ monitoring of APM through SPAMS, 150,389 single particles were sampled, and valid positive- and negative-ion mass spectra were acquired for 6333 particles. The NFPM and LDPM collected from the arboretum were successfully analyzed using PMRC with SPAMS. In SPAMS, 10,177 and 40,418 single particles of NFPM and LDPM, respectively, were sampled, with valid positive- and negative-ion mass spectra obtained for 1186 and 4528 particles of NFPM and LDPM, respectively. The analysis included size distributions, chemical compositions, and particle sources.

3.1. Particle size profiles

The size distributions generated by the PMRC of APM, NFPM, and LDPM samples are depicted in Fig. 3. These particles predominantly ranged between 0.2 and 2.0 μm in aerodynamic diameter. For APM and NFPM, the size distribution peaked between 0.5 and 0.7 μm (Fig. 3a and b). Notably, the peak patterns of APM differed significantly from NFPM, with APM exhibiting narrower and more pronounced peaks. This distinction indicates that APM tends to be more uniform in size compared to NFPM. Furthermore, the average particle size (D_c) for NFPM was calculated as 0.74 μm, slightly larger than that of APM, suggesting a propensity for slightly larger particles to settle naturally.

LDPM (Fig. 3c–f) displayed distinct peak patterns compared to NFPM, implying differences in deposition processes and potential
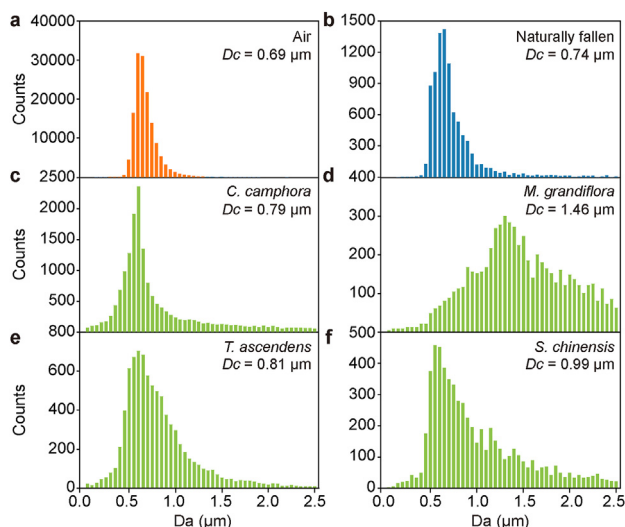
Fig. 3. Distribution of aerodynamic diameter of PM samples. The histograms depict particle counts versus aerodynamic diameter (Da) for various types of PM: **a**, APM; **b**, NFPM; **c**–**f**, LDPM particles. LDPM particles are collected from *Cinnamomum camphora* (**c**), *Magnolia grandiflora* (**d**), *Taxodium ascendens* (**e**), and *Sabina chinensis* (L.) Ant. "*Kaizuca*" (**f**). The average particle diameter (Dc) for each sample is calculated using equation (1), where Dc represents the mean diameter determined by integrating the product of the particle size and quantity over the size range normalized by the integral of the corresponding particle quantity.

surface modifications during the transition from deposition to settlement. Specifically, the PM deposited on the leaves of *C. camphora*, *M. grandiflora*, *T. ascendens*, and *S. chinensis* had average sizes of 0.79, 1.46, 0.81, and 0.99 μm, respectively. In other words, LDPM was 6.8−97.3 % larger in size than NFPM, a phenomenon that can be attributed to several underlying mechanisms. This could have been facilitated by the leaf's microenvironment [23], where factors such as the leaf's moisture, biochemical compounds, and surface texture create conditions conducive to particle adsorption and fusion [16]. Additionally, the presence of epicuticular waxes and the specific morphology of leaf surfaces might have played a significant role in trapping and merging airborne particles [28], leading to the observed increase in size.

The larger size of LDPM compared with APM is consistent with the findings from an urban park in Terni, Italy, by Sgrigna et al. [23] and in an urban green space in Hangzhou, China, by Wang et al. [25], who found large quantities and proportions of particles larger than 2.5 and 10 μm using SEM and elution−filtration−weighing methods, respectively (Table 2). Notably, Xu et al. [26] observed larger fractions in an artificial experiment in Beijing, which could be attributed to different environmental conditions and experimental setups. In contrast, the results showed a smaller average size compared to those from a smog chamber experiment by Yin et al. [27], who reported average sizes of 3.3−3.8 and 3.7−3.8 μm through sweep-resuspension-particle size spectrometry and X-ray microscope analysis, respectively. These discrepancies may be due to a variety of factors, including the priority of injection of fine particles (e.g., 0.2−2.0 μm) by SPAMS [39]. Future studies may focus on standardizing measurement techniques and consider local environmental variables to better understand the reasons behind these varying results.

3.2. Mass spectral signatures

Fig. 4 illustrates the average mass spectra of APM (Fig. 4a), NFPM (Fig. 4b), and LDPM (Fig. 4c−f). Represented by positive and negative peaks, these spectra provide insights into the molecular composition of the particles. Dominant signals in the positive-ion spectra are mostly attributed to crustal components such as K+ ($m/z = 39$), Na+ ($m/z = 23$), and Al+ ($m/z = 27$), while the negative-ion spectra predominantly feature components such as nitrite (NO$_2^-$: $m/z = -46$) and nitrate (NO$_3^-$: $m/z = -62$).

Despite originating from the same location, the PM components in different environmental media displayed marked differences. For instance, Al+, Ca+, Fe+, and silicates such as SiO$_2^-$ and SiO$_3^-$ exhibited higher peak intensities in LDPM compared to APM and NFPM. This variation provides insights into how particle composition transforms from an airborne state to deposition on leaf surfaces, which may be attributed to the physical characteristics of leaves, including surface roughness or the presence of epicuticular waxes [28] that enhance the adherence of these particles [42]. In contrast, HSO$_4^-$ and EC showed the highest relative intensities in APM, with a decreasing trend observed in NFPM and LDPM. This could be indicative of processes such as decomposition by microbial activities, which are more likely to affect particles once they settle on leaf surfaces [43].

To verify the reproducibility of the mass spectral features, 2 p.m. samples from the same underlying surface (the leaves of *M. grandiflora*) were repetitively measured using the PMRC-SPAMS system. The average mass spectra for these samples were obtained (Fig. S3, Supplementary Materials), and they closely matched the measurement results (Fig. 4d). This result indicates the stability and reproducibility of the PMRC-SPAMS system for the analysis of surface-deposited particles.

Further analysis of minor signals (with a relative peak intensity below 0.01, as shown in the insets of each panel in Fig. 4) revealed more distinct patterns. The positive-ion spectra mainly included peaks corresponding to EC (C$_n^+$, n = 1, 2, 3, 5, and 7), OC (C$_2$H$_5^+$, C$_2$H$_3$O+, C$_3$H$_3^+$, C$_3$H$_6^+$, C$_3$H$_6$O$_2^+$, C$_7$H$_5$O+, C$_8$H$_5$O$_3^+$, and arene), HMs (e.g., Pb+, Cu+, Ni+, and Cr+), and certain crustal components (Si+, Fe+, Ca+, Ti+, and Li+). The negative-ion spectra mainly contained peaks corresponding to EC (C$_n^-$, n = 1, 5, 6, and 7), OC (C$_2$H$_3^-$, C$_2$HO$^-$, C$_3$H$_4^-$, C$_4$H$^-$, C$_4$H$_2^-$, C$_5$H$_6^-$, and C$_6$H$_5$COO$^-$), secondary sulfate components (SO$_3^-$, HSO$_3^-$, SO$_4^-$, and HSO$_4^-$), phosphate (PO$_3^-$), levoglucosan (LEV; $m/z = -45, -59, -71$, and -73), and halogen ions (Cl$^-$). Notably, except for K+, which was sensitive to SPAMS, EC, secondary products (NO$_3^-$, NO$_2^-$, NH$_4^+$, SO$_4^-$, HSO$_4^-$, and HSO$_3^-$), and some OC compounds (C$_3$H$_3^+$, C$_5$H+, C$_5$H$_6^-$, and arene) were the main components of APM (Fig. 4a). In contrast, OC dominated the NFPM spectra (positive-ion spectra: C$_3$H$_3^+$, C$_3$H$_6^+$, C$_5$H+, C$_7$H$_5$O+, and C$_8$H$_5$O$_3^+$; negative-ion spectra: C$_5$H$_6^-$, C$_2$H$_3^-$, C$_2$HO$^-$, CH$_3$CO$^-$, and C$_6$H$_5$COO$^-$). The dominance of OC in NFPM spectra may reflect an accumulation of organic materials through natural processes [44].

The LDPM spectra showed higher intensities for crustal components (Si+, HSiO$_3^-$, Fe+, and Ti+) and LEV than the APM and NFPM spectra. Moreover, differences in LEV, HMs, and some OC compounds were observed among different tree species, suggesting species-specific influences on the chemical makeup of deposited particles. For example, the PM deposited on *C. camphora* showed considerably higher signal intensities for LEV ($m/z = -45, -59, -71$, and -73) and contained a large quantity of Pb+-rich components, unlike that on *M. grandiflora*. These findings imply that different plant species influence the chemical makeup of deposited particles differently. This could be due to the unique surface properties of the leaves of each species, affecting how particles adhere and react upon deposition [45].

3.3. Composition classification

Based on the similarities of mass-to-charge ions and the intensities of mass spectral peaks, a multitude of ionized particles were systematically categorized into several clusters using the ART-

Table 2
Comparisons of this study with other studies reporting the size of PM accumulating on leaf surfaces.

Study area	Method	Size fractions	Reference
An arboretum in Shanghai, China	Sweep-resuspension- SPAMS	Average size of 0.8−1.5 μm	This study
An urban park in the industrial city of Terni, Italy	SEM	PM_1 (0.4 μg cm^{-2}) $PM_{2.5}$ (1.3 μg cm^{-2}) PM_{10} (5.2 μg cm^{-2})	[23]
	Vacuum filtration	$PM_{2.5}$ (1.3 μg cm^{-2}) PM_{10} (3.1 μg cm^{-2})	
An urban green space on a campus in Hangzhou, China	Elution-filtration-weighing	$PM_{2.5}$ (5−21 %), $PM_{2.5-10}$, (11−40 %) PM_{10-100} (49−83 %)	[25]
An artificial experiment in Beijing, China	Elution-filtration- weighing	$PM_{0.2-3}$ (0.6−10.3 μg cm^{-2}) PM_{3-10} (1.0−18.8 μg cm^{-2}) PM_{10-100} (4.5−60.1 μg cm^{-2})	[26]
A smog chamber experiment in Shanghai, China	Sweep-resuspension- particle size spectrometry	PM_1 (14−18 %) $PM_{1-2.5}$ (28−29 %) $PM_{2.5-5}$ (34−37 %) Average size of 3.3−3.5 μm	[27]
	X-ray microscope	Average size of 3.7−3.8 μm	

2a neural network algorithm. This advanced classification yielded 148 clusters for APM and 80 clusters for NFPM, as well as 47−76 clusters for the single particles of LDPM samples, with both positive- and negative-ion spectra considered. Notably, the predominant clusters, encompassing the first 65 for APM and 49 for NFPM, accounted for over 95 % of the ionized particles in these samples. Similarly, for the LDPM samples from *C. camphora*, *M. grandiflora*, *T. ascendens*, and *S. chinensis*, the primary 42, 40, 24, and 39 clusters, respectively, encompassed the majority of the ionized particles. Nevertheless, the clusters delineated by the ART-2a algorithm were not sufficiently distinct, with some demonstrating only marginal differences in specific spectral intensities. Therefore, manual classification was necessary to amalgamate similar clusters. This was conducted according to the predominant chemical compositions identified within the mass spectra, as suggested by Xu et al. [15] and Hu et al. [35], ensuring a more robust categorization of particle types. The final particle categories included EC, OC, ECOC, Na-rich, K-rich, HMs, LEV, Crust, Secondary reaction products (Sec), and Others (Fig. 5).

APM was primarily composed of EC (19.9 %), OC (17.1 %), and Sec (12.8 %), reflecting the influence of anthropogenic activities, such as combustion and industrial processes. In contrast, NFPM predominantly contained OC (31.2 %), K-rich compounds (19.1 %), and Na-rich compounds (10.9 %), pointing to a composition influenced by natural sources and perhaps agricultural activities. The LDPM samples, however, were markedly dominated by Crust, with 54.5 %, 60.6 %, 53.9 %, and 56.6 % of the PM on the foliage of *C. camphora*, *M. grandiflora*, *T. ascendens*, and *S. chinensis*, respectively (Fig. 5a). Specifically, Al^+, Ca^+, Fe^+, Ti^+, O^-, SiO_2^-, SiO_3^-, and PO_3^- were the main ions in LDPM, as revealed by the spectral signatures. The mass spectra presented in Fig. S4 (Supplementary Materials) clearly show that the chemical composition of the Crust category was not the same as that of the Earth's crust, which mainly consists of elements such as O, Si, Al, Fe, Ca, K, and Na. However, all these elements could be observed in the mass spectra of the Crust category (Fig. S4, Supplementary Materials). Leaves hanging in a well-ventilated environment may contribute to their ability to capture suspended dust particles from the ground by wind [46]. Therefore, the predominance of crustal dust in LDPM indicates that leaves can serve as a significant sink for geogenic materials, potentially mitigating the impact of soil erosion and dust storms on air quality [47].

Hierarchical cluster analysis underscored a distinct divergence in chemical composition among APM, NFPM, and LDPM. This divergence suggests that the chemical components of deposited particles are highly influenced by the nature of the underlying surface. The subdivision of LDPM into two subgroups was noteworthy, with the groups corresponding to the particles collected from coniferous species and broad-leaved species. This distinction clearly emphasizes the impact of different vegetation types on the compositional profile of deposited PM. The chemical makeup of particles deposited on leaves may be affected by various factors, including leaf morphology, surface wax composition, age of needles/leaves, and the presence of biological compounds that can alter the composition of accumulated PM [48].

The analysis also probed the variation in PM composition as a function of particle size, segmented at 0.5 μm intervals. In the case of APM (Fig. 5b), EC, and ECOC predominantly constituted PM fractions within the 0−1.0 μm size range. LEV and HM content peaked within the intermediate size range of 1.0−1.5 μm, which may suggest their origin from specific combustion processes, such as biomass burning, that emit particles of this size range [49]. These components were diminished in larger particles, possibly due to the gravitational settling that preferentially affects heavier and larger particulates. Conversely, the proportion of crustal particles showed an increase with particle size, dominating the PM fraction in the range of 1.5−2.5 μm. The prominence of Crust in larger APM fractions contrasts with the distribution of EC, potentially due to the different sources and transport mechanisms. Larger particles are typically less influenced by atmospheric chemistry and more influenced by mechanical processes, such as the resuspension of road dust and soil [50].

Regarding NFPM (Fig. 5c), OC, K-rich compounds, and EC were the principal components of submicron particles (0−1.0 μm). The substantial presence of OC in NFPM could be indicative of natural emissions from plants themselves and the decomposition of organic matter, which tends to produce finer particles [51]. HMs and Na-rich particles, peaking at a size of 1.0−1.5 μm, subsequently decreased in abundance in larger particles. Conversely, the presence of LEV and Crust escalated with particle size. These observations align with a study reporting the elevated presence of silicates in larger particles from coal-powered plant emissions [15].

For all leaf-deposited particulate matter (Fig. 5d−g), Crust consistently dominated, indicating that leaf surfaces effectively trap particles of various sizes, particularly larger crustal elements.
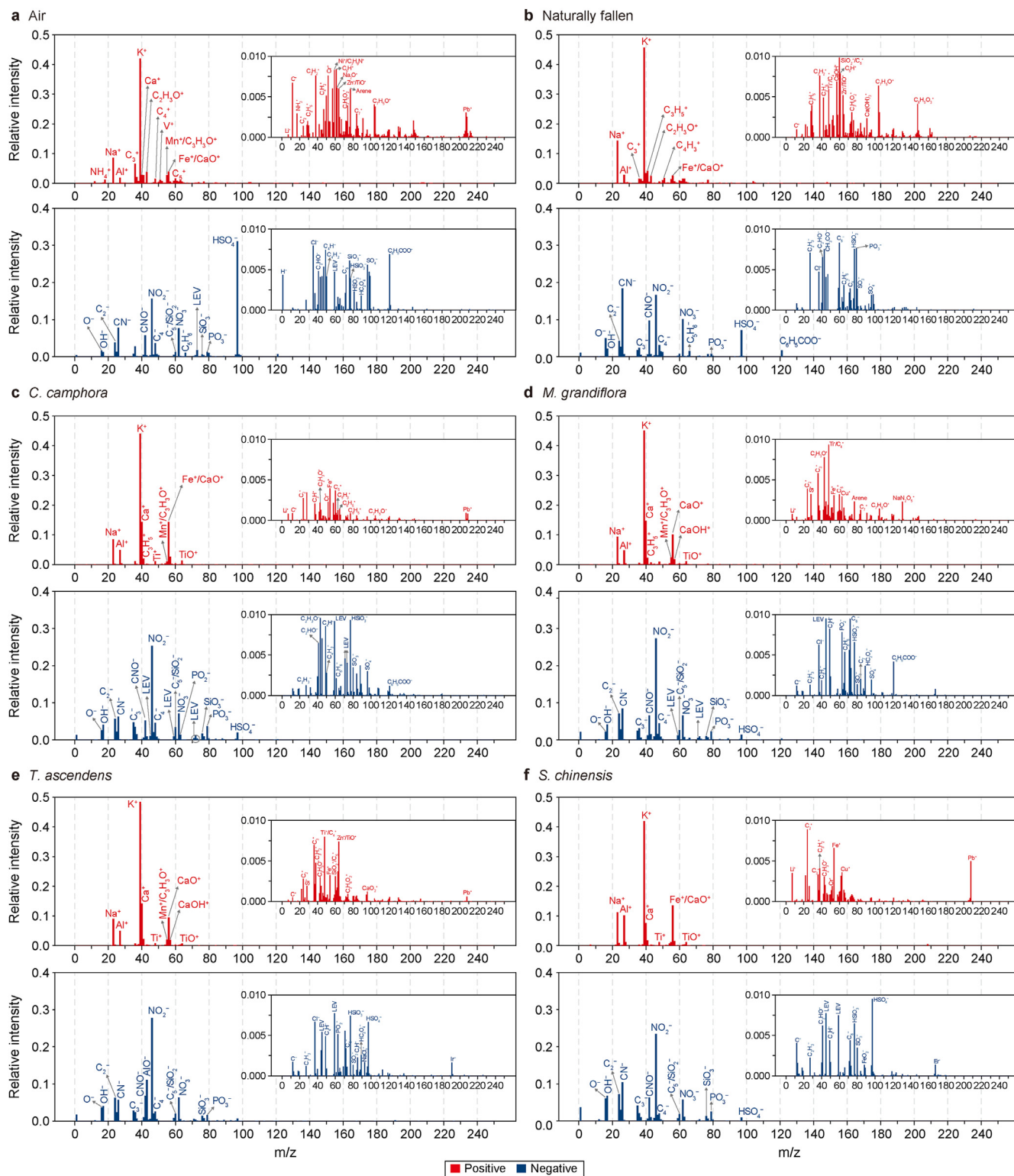
Fig. 4. Average mass spectral features of PM samples. **a**, APM; **b**, NFPM; **c**, *C. camphora*; **d**, *M. grandiflora*; **e**, *T. ascendens*; **f**, *S. chinensis*. The horizontal axis denotes the mass-to-charge ratio (m/z), and the vertical axis quantifies the relative intensity of the detected signals by SPAMS. The positive (red) and negative (blue) peaks correspond to the positively and negatively charged ions identified in the particles.

The composition variation between coniferous and broad-leaved species highlights the impact of leaf surface properties on particle deposition. A recent study showed that the surface free energy of the leaves of *T. ascendens* and *S. chinensis* was considerably higher than that of the leaves of *C. camphora* and *M. grandiflora*, which indicates that the leaves of *T. ascendens* and *S. chinensis* have a higher affinity for the retention of PM with OC fractions than those of *C. camphora* and *M. grandiflora* [37]. Thus, surface-free energy is
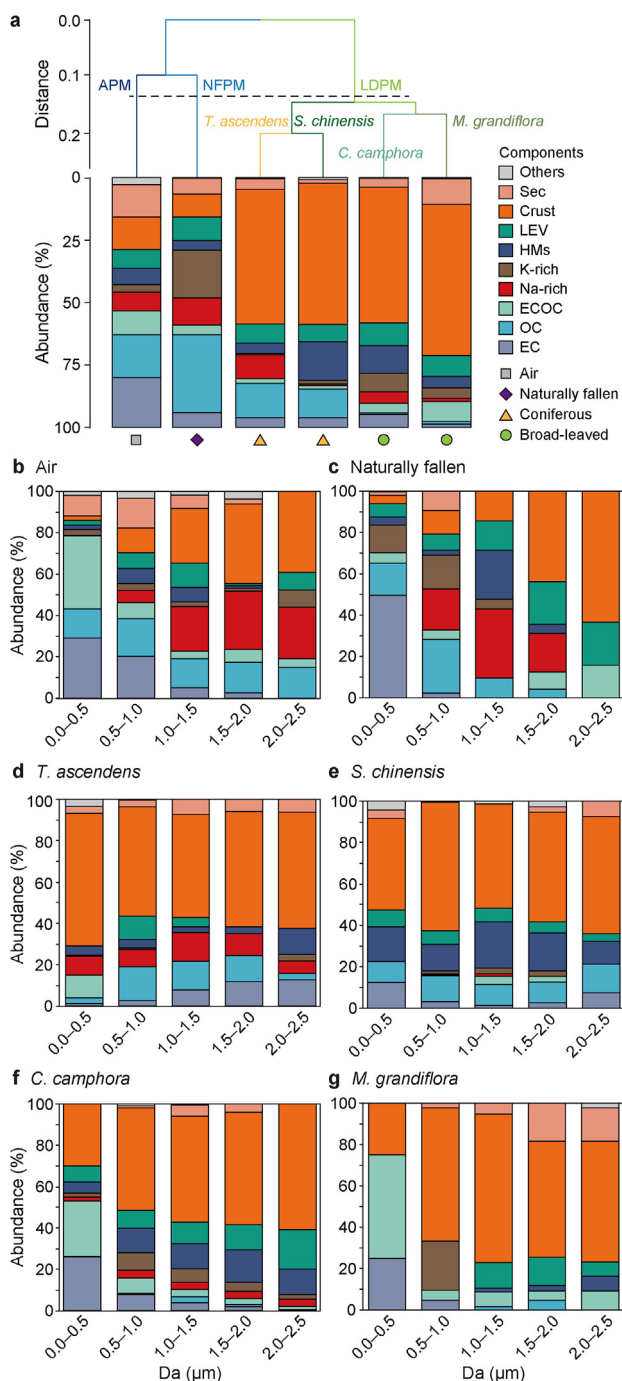
Fig. 5. The chemical composition of PM samples. **a**, The composition characteristics and clustering characteristics of particles from APM, NFPM, and LDPM. The figure categorizes the components into ten distinct types: elemental carbon (EC), organic carbon (OC), a combination of EC and OC (ECOC), sodium-rich (Na-rich), potassium-rich (K-rich), heavy metals (HMs), levoglucosan (LEV), crustal species (Crust), secondary reaction products (Sec), and others. K-means clustering based on the average linkage method was applied to characterize the compositional differences of APM, NFPM, and LDPM. **b**–**g**, Chemical compositions along particle sizes for the APM (**b**), NFPM (**c**), PM deposited on *T. ascendens* (**d**), *S. chinensis* (**e**), *C. camphora* (**f**), and *M. grandiflora* (**g**). The horizontal axis denotes particle size (D$_a$), and the vertical axis illustrates the relative abundance of each component within the PM.
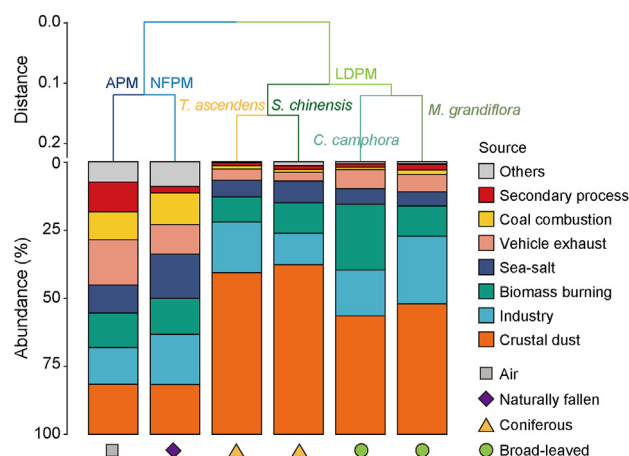
Fig. 6. Sources of various types of PM: APM, NFPM, and LDPM. The figure categorizes the sources into eight distinct types: crustal dust, industry, biomass burning, sea salt, vehicle exhaust, coal combustion, secondary process, and others. K-means clustering based on the average linkage method was applied to characterize the source differences of APM, NFPM, and LDPM.

3.4. Source apportionment

To further elucidate the compositional diversity of APM, NFPM, and LDPM, a receptor model based on aerosol mass spectra was utilized to classify ionized particles and uncover their source information [38]. Specifically, based on the monitoring results and referring to the Technical Guide for the Sources Analysis of Particulate Matter, combined with the industrial structure and energy consumption in Shanghai, the sources of PM pollution were categorized into eight distinct groups: vehicle exhaust, coal combustion, biomass burning, industrial emissions, crustal dust, sea salt, secondary generations, and others [52]. Fig. 6 visually articulates the source profiles for APM, NFPM, and LDPM.

APM exhibited a heterogeneous source distribution. The proportions of crustal dust and vehicle exhaust were notably substantial, accounting for 18.4 % and 16.5 %, respectively, indicating that urban atmospheric dynamics are heavily influenced by anthropogenic sources [14]. Industrial emissions, biomass burning, secondary processes, and sea salt also contributed significantly, with each ranging from 10.3 % to 13.4 %. NFPM sources were led by industrial emissions and crustal dust, each constituting 18.3 %, followed by sea salt, at 16.3 %. Biomass burning and coal combustion, as contributors, hint at ongoing energy production and agricultural practices affecting PM that settle naturally [53]. LDPM source analysis revealed that crustal dust was a predominant source across species, suggesting the strong influence of the physical process of dry deposition [29], in which soil-derived particles are effectively captured by leaf surfaces.

The source clustering for LDPM, denoted by geometric shapes for coniferous and broad-leaved species, underpins the modulatory effect of vegetation type on particle deposition. This finding aligns with the hierarchical clustering analysis of PM chemical composition presented in Section 3.3. The broader leaf surfaces of species such as *C. camphora* and *M. grandiflora* can offer a distinct interaction profile with PM compared to the needle-like leaves of coniferous species such as *T. ascendens* and *S. chinensis*, potentially leading to distinct chemical compositions of the deposited particles [54].

3.5. Practical implications of the study

The findings offer valuable practical applications for urban air quality management by harnessing the natural filtration

likely to influence the interactions of PM components and leaf epicuticular waxes, thereby potentially affecting the composition of deposited PM particles.

capabilities of specific tree species. The observed differences in particle size between LDPM and APM suggest that urban vegetation, particularly species such as *M. grandiflora*, demonstrates a preference for capturing larger airborne particulates, a feature that can be utilized to improve air quality in urban landscapes. Furthermore, the dominance of Crust in LDPM suggests that leaves are effective at trapping geogenic materials, thereby serving as a critical sink that may mitigate the repercussions of soil erosion and dust storms on urban air quality.

Moreover, the demonstrated efficiency of *S. chinensis* and *C. camphora* in capturing HMs and LEV, respectively, highlights their potential role in urban greening programs to mitigate pollution from specific PM components. Source apportionment analysis further informs the selection of vegetation for green spaces by identifying which tree species are most effective against specific pollution sources, such as vehicle exhaust or biomass burning [55]. Such a species-specific approach to urban forestry can enhance the understanding of the natural air filtration provided by trees for city planners and environmentalists in the placement in urban landscapes [56], allowing for the design of green spaces that target the predominant PM sources in particular urban areas.

3.6. Uncertainty and limitations of the study

First, while robust, the methodology employed in the current study to compare resuspended and native airborne particles faces challenges. Notably, atmospheric particle measurements were not conducted at the exact leaf collection sites. Instead, air sampling conducted on a monitoring station rooftop helped mitigate the possibility of the resuspension of particles from leaves into the air samples, thereby reducing the risk of cross-contamination. Additionally, there was a temporal variation in the sampling. APM was measured continuously during daylight hours for 6−8 h per day, while LDPM and NFPM were collected over a prolonged period and then determined. Given that all PM samples were collected over the same seven-day period, a reasonable degree of comparability can be assumed.

Second, while the pooled PM samples provided a representation of the particle size and chemical composition for each sample type, they also highlighted the challenge in quantifying variability between samples. Given the large number of particles analyzed in each pooled sample by SPAMS, the data largely represent the particle characteristics of LDPM, NFPM, and APM, as revealed by similar studies on brake wear−derived particles by Liu et al. [36]. Future work will include a comprehensive analysis of variability within tree species to more accurately estimate the species' capacity to retain different components in PM.

Additionally, there are some uncertainties concerning the particle size measurements of APM, NFPM, and LDPM. The resuspension process in the PMRC may have altered the size distribution of the adsorbed particles. As noted by Terzaghi et al. [56], resuspension can disaggregate particle clusters, possibly leading to the underrepresentation of larger particle aggregates originally present on leaf surfaces. Previous research has noted insignificant differences in particle size (Table 2) on leaf surfaces between X-ray microscopy observation and the sweep-resuspension method [27], further supporting the reliability of the findings in this study. This also suggests that there is a need for further research on particle coagulation mechanisms on leaf surfaces through controlled experimental methods.

4. Conclusions and prospects

This study revealed that LDPM is 6.8−97.3 % larger in size than NFPM. NFPM was primarily composed of OC and K-rich

components, while LDPM displayed the dominance of Crust, HMs, and LEV. Source apportionment analysis showed that NFPM predominantly originated from industrial emissions and sea salt, in contrast to LDPM, which was largely derived from crustal dust, industrial emissions, and biomass burning. These observed differences in particle size and composition can be linked to the ventilated conditions around the leaves and the biochemical properties of their surfaces. Consequently, the distinct chemical profiles and particle clustering highlight the transformational impact of vegetative surfaces, reflecting anthropogenic and natural sources. This enhanced understanding of the role of urban greenery offers valuable insights for air quality management, underscoring the need to consider species-specific influences on PM when planning to maximize air purification benefits.

An important future direction would be to investigate the trajectories of PM to evaluate the influence of external sources at the city or country level [18]. This analysis would help distinguish between local and broader environmental impacts on PM deposition. Furthermore, research could concentrate on the temporal dynamics of particle deposition, examining how seasonal variations and meteorological conditions influence the ability of different tree species to retain specific particulate components. Another focus would be on understanding the impact of leaf surface properties, particularly surface morphology and epicuticular composition, on the size and chemical composition of adsorbed particles. This focused approach would enhance the understanding of the interaction dynamics between particulates and different vegetation types, thereby contributing to the development of effective urban greening strategies.

Declaration of competing interest

The authors declare that they have no known competing financial interests or personal relationships that could have appeared to influence the work reported in this paper.

CRediT authorship contribution statement

Dele Chen: Conceptualization, Investigation, Methodology, Software, Validation, Visualization, Writing − original draft, Writing − review & editing. **Hua-Yun Xiao:** Writing − review & editing. **Ningxiao Sun:** Investigation, Writing − review & editing. **Jingli Yan:** Validation, Writing − review & editing. **Shan Yin:** Conceptualization, Funding acquisition, Methodology, Project administration, Supervision, Writing − review & editing.

Declaration of competing interest

The authors declare that they have no known competing financial interests or personal relationships that could have appeared to influence the work reported in this paper.

Appendix A. Supplementary data

Supplementary data to this article can be found online at https://doi.org/10.1016/j.ese.2024.100432.

References

[1] Y. Qi, S. Wei, T. Xin, C. Huang, Y. Pu, J. Ma, C. Zhang, Y. Liu, I. Lynch, S. Liu, Passage of exogeneous fine particles from the lung into the brain in humans and animals, Proc. Natl. Acad. Sci. USA 119 (26) (2022) e2117083119.

[2] B. Panessa-Warren, T. Butcher, J.B. Warren, R. Trojanowski, K. Kisslinger, G. Wei, Y. Celebi, Wood combustion nanoparticles emitted by conventional and advanced technology cordwood boilers, and their interactions in vitro with human lung epithelial monolayers, Biofuel Res. J. 9 (3) (2022) 1659–1671.

[3] K.R. Daellenbach, G. Uzu, J. Jiang, L.-E. Cassagnes, Z. Leni, A. Vlachou, G. Stefenelli, F. Canonaco, S. Weber, A. Segers, Sources of particulate-matter air pollution and its oxidative potential in Europe, Nature 587 (7834) (2020) 414–419.

[4] B. Wang, Y.-S. Lau, Y. Huang, B. Organ, H.-C. Chuang, S.S.H. Ho, L. Qu, S.-C. Lee, K.-F. Ho, Chemical and toxicological characterization of particulate emissions from diesel vehicles, J. Hazard Mater. 405 (2021) 124613.

[5] Y. Hao, X. Meng, X. Yu, M. Lei, W. Li, W. Yang, F. Shi, S. Xie, Quantification of primary and secondary sources to PM$_{2.5}$ using an improved source regional apportionment method in an industrial city, China, Sci. Total Environ. 706 (2020) 135715.

[6] M. Xu, Z. Liu, B. Hu, G. Yan, J. Zou, S. Zhao, J. Zhou, X. Liu, X. Zheng, X. Zhang, Chemical characterization and source identification of PM$_{2.5}$ in Luoyang after the clean air actions, J. Environ. Sci. 115 (2022) 265–276.

[7] S.E. Sbai, C. Li, A. Boreave, N. Charbonnel, S. Perrier, P. Vernoux, F. Bentayeb, C. George, S. Gil, Atmospheric photochemistry and secondary aerosol formation of urban air in Lyon, France, J. Environ. Sci. 99 (2021) 311–323.

[8] L.-H. Rivellini, M.G. Adam, N. Kasthuriarachchi, A.K.Y. Lee, Characterization of carbonaceous aerosols in Singapore: insight from black carbon fragments and trace metal ions detected by a soot particle aerosol mass spectrometer, Atmos. Chem. Phys. 20 (10) (2020) 5977–5993.

[9] M. Stafoggia, B. Oftedal, J. Chen, S. Rodopoulou, M. Renzi, R.W. Atkinson, M. Bauwelinck, J.O. Klompmaker, A. Mehta, D. Vienneau, Long-term exposure to low ambient air pollution concentrations and mortality among 28 million people: results from seven large European cohorts within the ELAPSE project, Lancet Planet. Health 6 (1) (2022) e9–e18.

[10] R. Pace, G. Guidolotti, C. Baldacchini, E. Pallozzi, R. Grote, D.J. Nowak, C. Calfapietra, Comparing i-Tree eco estimates of particulate matter deposition with leaf and canopy measurements in an urban mediterranean Holm Oak Forest, Environ. Sci. Technol. 55 (10) (2021) 6613–6622.

[11] D. Han, H. Shen, W. Duan, L. Chen, A review on particulate matter removal capacity by urban forests at different scales, Urban For. Urban Green. 48 (2020) 126565.

[12] J. Liu, J. Zhai, L. Zhu, Y. Yang, J. Liu, Z. Zhang, Particle removal by vegetation: comparison in a forest and a wetland, Environ. Sci. Pollut. Res. 24 (2) (2017) 1597–1607.

[13] C. Giorio, A. Tapparo, M. Dall'Osto, D.C. Beddows, J.K. Esser-Gietl, R.M. Healy, R.M. Harrison, Local and regional components of aerosol in a heavily trafficked street canyon in central London derived from PMF and cluster analysis of single-particle ATOFMS spectra, Environ. Sci. Technol. 49 (6) (2015) 3330–3340.

[14] J. Yang, S. Ma, B. Gao, X. Li, Y. Zhang, J. Cai, M. Li, B. Huang, M. Zheng, Single particle mass spectral signatures from vehicle exhaust particles and the source apportionment of on-line PM$_{2.5}$ by single particle aerosol mass spectrometry, Sci. Total Environ. 593 (2017) 310–318.

[15] J. Xu, H. Wang, X. Li, Y. Li, J. Wen, J. Zhang, X. Shi, M. Li, W. Wang, G. Shi, Refined source apportionment of coal combustion sources by using single particle mass spectrometry, Sci. Total Environ. 627 (2018) 633–646.

[16] N. Ha, E. Seo, S. Kim, S.J. Lee, Adsorption of nanoparticles suspended in a drop on a leaf surface of *Perilla frutescens* and their infiltration through stomatal pathway, Sci. Rep. 11 (1) (2021) 11556.

[17] J. Liu, Z. Cao, S. Zou, H. Liu, X. Hai, S. Wang, J. Duan, B. Xi, G. Yan, S. Zhang, An investigation of the leaf retention capacity, efficiency and mechanism for atmospheric particulate matter of five greening tree species in Beijing, China, Sci. Total Environ. 616 (2018) 417–426.

[18] M.N. Anwar, M. Shabbir, E. Tahir, M. Iftikhar, H. Saif, A. Tahir, M.A. Murtaza, M.F. Khokhar, M. Rehan, M. Aghbashlo, Emerging challenges of air pollution and particulate matter in China, India, and Pakistan and mitigating solutions, J. Hazard Mater. 416 (2021) 125851.

[19] Z. Fan, Y. Zhao, B. Hu, L. Wang, Y. Guo, Z. Tang, J. Tang, J. Ma, H. Gao, T. Huang, Enhancing urban real-time PM$_{2.5}$ monitoring in street canyons by machine learning and computer vision technology, Sustain. Cities Soc. 100 (2024) 105009.

[20] H. Hosseinzadeh-Bandbafha, H.K.S. Panahi, M. Dehhaghi, Y. Orooji, H. Shahbeik, O. Mahian, H. Karimi-Maleh, M.A. Kalam, G.S. Jouzani, C. Mei, Applications of nanotechnology in biodiesel combustion and post-combustion stages, Renew. Sustain. Energy Rev. 182 (2023) 113414.

[21] M. Budaniya, A.C. Rai, Effectiveness of plants for passive removal of particulate matter is low in the indoor environment, Build. Environ. 222 (2022) 109384.

[22] T. Ysebaert, K. Koch, R. Samson, S. Denys, Green walls for mitigating urban particulate matter pollution—a review, Urban For. Urban Green. 59 (2021) 127014.

[23] G. Sgrigna, C. Baldacchini, S. Dreveck, Z. Cheng, C. Calfapietra, Relationships between air particulate matter capture efficiency and leaf traits in twelve tree species from an Italian urban-industrial environment, Sci. Total Environ. 718 (2020) 137310.

[24] U. Weerakkody, J.W. Dover, P. Mitchell, K. Reiling, Topographical structures in planting design of living walls affect their ability to immobilise traffic-based particulate matter, Sci. Total Environ. 660 (2019) 644–649.

[25] M. Wang, M. Qin, P. Xu, D. Huang, X. Jin, J. Chen, D. Dong, Y. Ren, Atmospheric particulate matter retention capacity of bark and leaves of urban tree species, Environ. Pollut. 342 (2024) 123109.

[26] X. Xu, X. Yu, L. Bao, A.R. Desai, Size distribution of particulate matter in runoff from different leaf surfaces during controlled rainfall processes, Environ. Pollut. 255 (2019) 113234.

[27] S. Yin, J. Lyu, X. Zhang, Y. Han, Y. Zhu, N. Sun, W. Sun, C. Liu, Coagulation effect of aero submicron particles on plant leaves: measuring methods and potential mechanisms, Environ. Pollut. 257 (2020) 113611.

[28] S. Chen, H. Yu, X. Teng, M. Dong, W. Li, Composition and size of retained aerosol particles on urban plants: insights into related factors and potential impacts, Sci. Total Environ. 853 (2022) 158656.

[29] T.-H. Su, C.-S. Lin, J.-C. Lin, C.-P. Liu, Dry deposition of particulate matter and its associated soluble ions on five broadleaved species in Taichung, central Taiwan, Sci. Total Environ. 753 (2021) 141788.

[30] C. Baldacchini, A. Castanheiro, N. Maghakyan, G. Sgrigna, J. Verhelst, R. Alonso, J.H. Amorim, P. Bellan, D.Đ. Bojović, J.r. Breuste, How does the amount and composition of PM deposited on *Platanus acerifolia* leaves change across different cities in Europe? Environ. Sci. Technol. 51 (3) (2017) 1147–1156.

[31] H.-T. Bui, J. Park, E. Lee, M. Jeong, B.-J. Park, Particulate matter accumulation and elemental composition of eight roadside plant species, Urban Sci 7 (2) (2023) 51.

[32] M. Ristorini, M.L. Astolfi, M.A. Frezzini, S. Canepari, L. Massimi, Evaluation of the efficiency of *Arundo donax* L. leaves as biomonitors for atmospheric element concentrations in an urban and industrial area of central Italy, Atmosphere 11 (2020) 226.

[33] H. Xu, W. Wang, H. Wang, Y. Sun, Z. Zhong, S. Wang, Differences in quantity and composition of leaf particulate matter and morphological structures in three evergreen trees and their association in Harbin, China, Environ. Pollut. 252 (2019) 1772–1790.

[34] L. Li, Z. Huang, J. Dong, M. Li, W. Gao, H. Nian, Z. Fu, G. Zhang, X. Bi, P. Cheng, Real time bipolar time-of-flight mass spectrometer for analyzing single aerosol particles, Int. J. Mass Spectrom. 303 (2–3) (2011) 118–124.

[35] J. Hu, C. Xie, L. Xu, X. Qi, S. Zhu, H. Zhu, J. Dong, P. Cheng, Z. Zhou, Direct analysis of soil composition for source apportionment by laser ablation single-particle aerosol mass spectrometry, Environ. Sci. Technol. 55 (14) (2021) 9721–9729.

[36] J. Liu, J. Peng, Z. Men, T. Fang, J. Zhang, Z. Du, Q. Zhang, T. Wang, L. Wu, H. Mao, Brake wear-derived particles: single-particle mass spectral signatures and real-world emissions, Environ. Sci. Ecotechnol. 15 (2023) 100240.

[37] J. Lyu, D. Chen, X. Zhang, J. Yan, G. Shen, S. Yin, Coagulation effect of atmospheric submicron particles on plant leaves: Key functional characteristics and a comparison with dry deposition, Sci. Total Environ. 868 (2023) 161582.

[38] X. Peng, X. Liu, X. Shi, G. Shi, M. Li, J. Liu, Y. Huangfu, H. Xu, R. Ma, W. Wang, Source apportionment using receptor model based on aerosol mass spectra and 1 h resolution chemical dataset in Tianjin, China, Atmos. Environ. 198 (2019) 387–397.

[39] J. Xu, M. Li, G. Shi, H. Wang, X. Ma, J. Wu, X. Shi, Y. Feng, Mass spectra features of biomass burning boiler and coal burning boiler emitted particles by single particle aerosol mass spectrometer, Sci. Total Environ. 598 (2017) 341–352.

[40] X.-H. Song, P.K. Hopke, D.P. Fergenson, K.A. Prather, Classification of single particles analyzed by ATOFMS using an artificial neural network, ART-2A, Anal. Chem. 71 (4) (1999) 860–865.

[41] J. Sun, Y. Li, W. Xu, W. Zhou, A. Du, L. Li, X. Du, F. Huang, Z. Li, Z. Zhang, Single-particle volatility and implications for brown carbon absorption in Beijing, China, Sci. Total Environ. 854 (2023) 158874.

[42] S. Muhammad, K. Wuyts, G. Nuyts, K. De Wael, R. Samson, Characterization of epicuticular wax structures on leaves of urban plant species and its association with leaf wettability, Urban For. Urban Green. 47 (2020) 126557.

[43] M. Mandal, S. Das, A. Roy, R. Rakwal, O.A. Jones, R. Popek, G.K. Agrawal, A. Sarkar, Interactive relations between plants, phyllosphere microbial community, and particulate matter pollution, Sci. Total Environ. 890 (2023) 164352.

[44] A.S. Wozniak, J.E. Bauer, R.M. Dickhut, Fossil and contemporary aerosol particulate organic carbon in the eastern United States: implications for deposition and inputs to watersheds, Global Biogeochem. Cycles 25 (2011) GB2013.

[45] M.J. Kwak, J.K. Lee, S. Park, H. Kim, Y.J. Lim, K.-A. Lee, J.-a. Son, C.-Y. Oh, I. Kim, S.Y. Woo, Surface-based analysis of leaf microstructures for adsorbing and retaining capability of airborne particulate matter in ten woody species, Forests 11 (2020) 946.

[46] A. Garcia, E. Jones, A.S. Echt, R.M. Hall, An evaluation of an aftermarket local exhaust ventilation device for suppressing respirable dust and respirable crystalline silica dust from powered saws, J. Occup. Environ. Hyg. 11 (2014) D200–D207.

[47] S. Banerjee, A. Banerjee, D. Palit, Morphological and biochemical study of plant species-a quick tool for assessing the impact of air pollution, J. Clean. Prod. 339 (2022) 130647.

[48] K. Corada, H. Woodward, H. Alaraj, C.M. Collins, A. de Nazelle, A systematic review of the leaf traits considered to contribute to removal of airborne

particulate matter pollution in urban areas, Environ. Pollut. 269 (2021) 116104.

[49] M.G. Adam, P.T.M. Tran, N. Bolan, R. Balasubramanian, Biomass burning-derived airborne particulate matter in Southeast Asia: a critical review, J. Hazard Mater. 407 (2021) 124760.

[50] E. Stratigou, S. Dusanter, J. Brito, V. Riffault, Investigation of PM_{10}, $PM_{2.5}$, PM_1 in an unoccupied airflow-controlled room: how reliable to neglect resuspension and assume unreactive particles? Build. Environ. 186 (2020) 107357.

[51] G.-H. Yu, S. Park, K.-H. Lee, Source contributions and potential source regions of size-resolved water-soluble organic carbon measured at an urban site over one year, Environ. Sci.-Proc. Imp. 18 (2016) 1343−1358.

[52] L. Shao, P. Liu, T. Jones, S. Yang, W. Wang, D. Zhang, Y. Li, C.-X. Yang, J. Xing, C. Hou, A review of atmospheric individual particle analyses: methodologies and applications in environmental research, Gondwana Res. 110 (2022) 347−369.

[53] C. Zhang, Y. Zhang, X. Liu, Y. Liu, C. Li, Characteristics and source apportionment of $PM_{2.5}$ under the dual influence of the Spring Festival and the COVID-19 pandemic in Yuncheng city, J. Environ. Sci. 125 (2023) 553−567.

[54] P. Michopoulos, M. Kostakis, P. Koulelis, A. Bourletsikas, K. Kaoukis, V. Kavvadias, D. Arapakis, I. Pasias, N.S. Thomaidis, N. Liakopoulou, Cycling and status of boron in two forest types in Greece, Ann. For. Res. 66 (2023) 113−122.

[55] H. Wang, B.A. Maher, I.A.M. Ahmed, B. Davison, Efficient removal of ultrafine particles from diesel exhaust by selected tree species: implications for roadside planting for improving the quality of urban air, Environ. Sci. Technol. 53 (12) (2019) 6906−6916.

[56] E. Terzaghi, E. Wild, G. Zacchello, B.E. Cerabolini, K.C. Jones, A. Di Guardo, Forest filter effect: role of leaves in capturing/releasing air particulate matter and its associated PAHs, Atmos. Environ. 74 (2013) 378−384.